INFRARED THERMAL WAVE DETECTION OF INTERFACIAL DEBONDING DEFECTS OF THERMAL BARRIER COATINGS BASED ON NON-LINEAR FREQUENCY MODULATION

by

Qing-Ju TANG [a*], ***Tao ZHANG*** [a], ***Zhuo-Yan GU*** [a], ***and Chi-Wu BU*** [b]

[a] School of Mechanical Engineering, Heilongjiang University of Science and Technology, Harbin, China

[b] College of Light Industry, Harbin University of Commerce, Harbin, China

Original scientific paper
https://doi.org/10.2298/TSCI2301705T

In order to improve the reliability of detecting the debonding defects at the interface of thermal barrier coatings (TBC), a non-linear frequency modulated (NLFM) infrared thermal wave detection method is proposed. A NLFM infrared thermal wave detection system is built, and zirconia TBC specimens are prepared and tested. The effects of defect diameter, excitation power, initial frequency and termination frequency on the defect detection effect are analyzed. Three algorithms such as principal component analysis (PCA) are used to process the image sequence, and the signal-to-noise ratio (SNR) of each sequence processing algorithm is calculated and compared. The results show that the larger the diameter of the defect, the easier it is to be detected, and the appropriate adjustment of the excitation power or the reduction of the initial and termination frequencies is beneficial to the detection of defects. Compared with the other two algorithms, the PCA method is more effective for image sequence processing. It offers a reference for detecting debonding flaws at the TBC interface.

Key words: *thermal barrier coating, debonding defects, image sequence, non-linear frequency-modulated*

Introduction

The TBC are one of the three key technologies for turbine blades, and they are now widely used in the blades of various gas turbines because of their advantages of reducing blade surface temperature, improving blade oxidation resistance, and extending blade service life [1, 2]. During service, the effects of thermal growth oxide generation, corrosion of molten glassy deposits calcium-magnesium-alumina silicate (CMAS) and thermal expansion coefficient mismatch can lead to cracks or debonding spalling inside TBC [3]. Therefore, to ensure the performance of TBC, it is necessary to detect the debonding defects of TBC by means of infrared thermal wave non-destructive tool (NDT).

With the advantages of high reliability, non-contact, fast detection speed and large detection range, infrared thermal wave NDT technique is widely used in many fields such as aerospace, electric power and machinery, and has developed into an important NDT technique for material surface and near-surface defects, which has received more and more attention from scientific researchers [4, 5]. However, there are few studies on debonding defects of TBC using NLFM infrared thermal wave NDT technique.

* Corresponding author, e-mail: tangqingju@126.com

In this paper, we use NLFM infrared thermal wave inspection for the detection of debonding defects at the interface of TBC, and analyze the effects of defect diameter, excitation power, initial frequency and termination frequency on the defect detection effect. The infrared thermogram sequences are processed using PCA, discrete Fourier transform and total harmonic distortion method, and the SNR of each sequence processing algorithm is calculated and compared.

The NLFM-based infrared thermal wave detection test

The NLFM heat flow

The NLFM (logarithmically modulated) heat flow including both static and dynamic components can be written [6]:

$$q(t) = q_{\mathrm{m}} + q_{\mathrm{n}} = \frac{q_{\max}}{2}\left\{1+\cos\left[2\pi\left(\frac{T}{\ln\left(\dfrac{f_b}{f_a}\right)}\left(f_a\left(\frac{f_b}{f_a}\right)^{t/T} - f_a\right)\right)+\varphi_0\right]\right\},\ t\in[0,T] \tag{1}$$

where $q(t)$ [Wm^{-2}] is the specimen surface heat flow, $q_{\max}$ – the maximum heat flow on the TBC specimen's surface, q_m – the specimen surface heat flow static component, q_n – the specimen surface heat flow component, f_a [Hz] – the Chirp modulation signal initial frequency, f_b – the Chirp modulation signal termination frequency, and T – the Chirp modulation signal modulation time.

Construction of the test system

Figure 1 shows the constructed NLFM infrared thermal imaging test system. First, the initial frequency, termination frequency, scanning time, excitation power and other parameters are set on the computer, and the non-linear modulation signal is output to the dimmer through NI-USB6229BNC data acquisition card, and the dimmer controls the halogen lamp to apply modulated heat flow to the specimen according to the received signal. Collection of thermal radiation on specimen surface by infrared thermal imager and saved in real time on the computer in text file format, and the pre-processing, calculation and analysis of the later test data are done by MATLAB software.

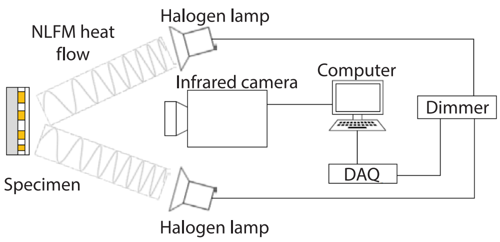

Figure 1. The NLFM infrared thermal imaging test system

Specimen preparation

The structure of TBC specimens is divided into three layers. The lower part is the matrix of GH4169 nickel base superalloy material, the middle part is the bonding layer of NiCoCrAlY material, and the top part is $ZrO_2 + 8\%wt.Y_2O_3$ ceramic layer. Specimen debonding defects are simulated using circular flat blind holes, and depths up to the lower surface of the ceramic top layer. As there are many defects, they are distributed evenly on the test piece as much as possible.

The effect of different parameters on the detection effect

Inspection tests were performed at room temperature and standard atmospheric pressure using the NLFM infrared thermal wave inspection system described previously and TBC prefabricated defect specimens by setting different test parameters. Compare the effects of different defect diameters, light source excitation power, initial and termination frequencies on the detection effect. The detection test parameters are shown in tab. 1.

Table 1. Test parameters for detecting debonding defects in TBC

Excitation power, P [W]	Original frequency, f_a [Hz]	Termination frequency, f_b [Hz]	Scanning time, T [second]	Sampling frequency [Hz]	Sampling time [second]
1600, 1800, 2000	0.1, 0.15, 0.2	0.05, 0.1, 0.2	20	20	40

The difference in surface temperature between the defect's center and the defect-free region is used as the evaluation criterion for the detection effect, and if the temperature at the center of the defect is T_2 and the temperature at the defect-free area is T_1, then the surface temperature difference T [°C] can be expressed:

$$\Delta T(0,t) = T_2 - T_1 = \frac{q_0}{\mathrm{e}\sqrt{\pi t}} \tag{2}$$

where q_0 is the energy absorbed by the surface of TBC and e – the thermal emissivity of the material.

Figures 2 and 3 is the effect curve of defect diameter and excitation power on surface temperature difference. As shown in fig. 2, due to the thermal insulation of TBC, the debonding defects accumulate more heat at the surface of TBC. Therefore, the larger is the diameter of TBC debonding defects, the larger is the temperature difference. As shown in fig. 3, the larger the excitation power, the larger the corresponding temperature difference, the more favorable to the detection of debonding defects.

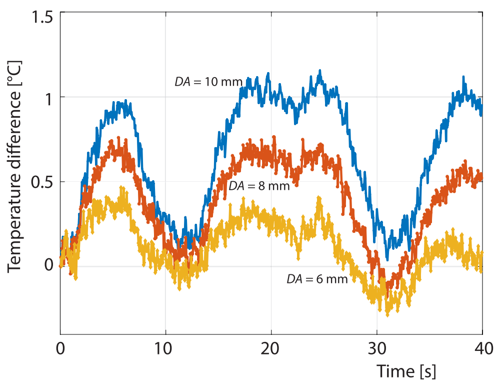

Figure 2. Effect of different defect diameters on surface temperature difference

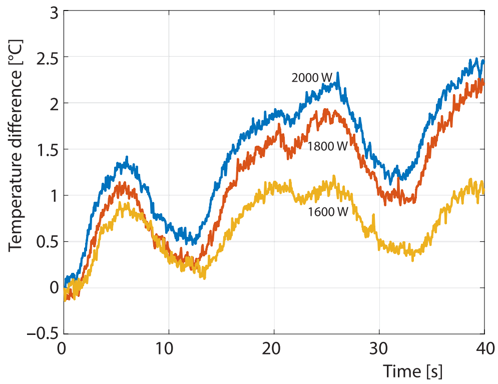

Figure 3. Effect of different excitation power on surface temperature difference

Figures 4 and 5 show the influence curves of different starting and ending frequencies on the surface temperature difference, respectively. The smaller is the initial frequency, the larger is the corresponding temperature difference. This is because the smaller is the modulation frequency, the higher is the average power of the thermal wave signal, the larger the surface temperature difference, and the better the defect detection effect. Similarly, the smaller the termination frequency, also corresponds to a larger temperature difference. Therefore, the smaller the initial frequency or the termination frequency used, the easier the defects are detected.

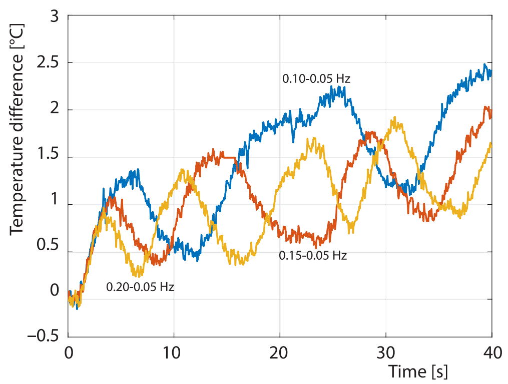

Figure 4. Effect of different initial frequencies on surface temperature difference

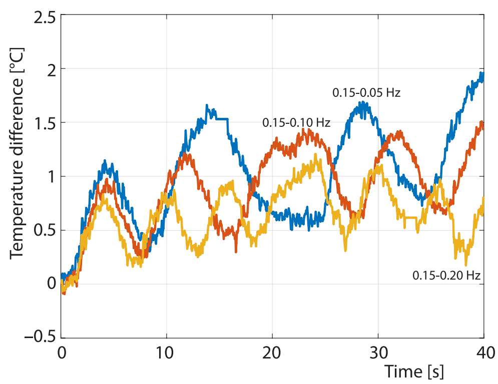

Figure 5. Effect of different termination frequencies on surface temperature difference

Image sequence processing

In order to make the test results under different parameters can be compared under the same magnitude, all test data are described:

$$p = \frac{p_0 - p_{\min}}{p_{\max} - p_{\min}} \tag{3}$$

where p is the normalized test data, p_0 – is test raw data, $p_{\min}$ – the minimum value, and $p_{\max}$ – the maximum value.

Principal component analysis method

The idea of PCA is to use the covariance matrix of the original data matrix to reconstruct the k-dimensional features based on the n-dimensional features, and map the n-dimensional features to the k-dimensional to achieve the effect of dimensionality reduction, thus transforming into a few comprehensive indicators, and the reconstructed k-dimensional orthogonal features are called principal components. The common method for calculating the covariance matrix by principal component analysis is singular value decomposition [7]. If A is an $m \times n$ matrix, we show that:

$$A = URV^T \tag{4}$$

where R is the diagonal matrix of the matrix A, U – the left singular vector of matrix A, and V – the right singular vector of matrix A.

Figure 6 shows the result of infrared thermogram processed by PCA.

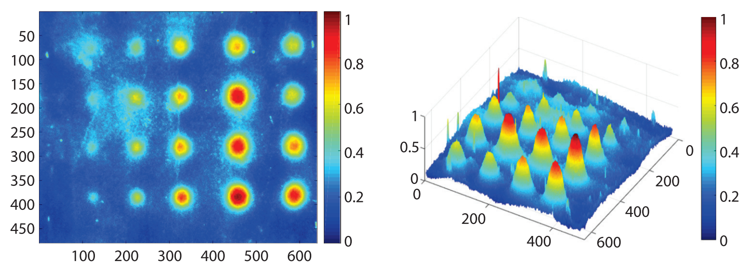

Figure 6. The result of infrared thermogram processed by PCA

Discrete Fourier transform

The discrete Fourier transform (DFT) provides a relatively simple method to analyze and study complex functions. After the original signal has been transformed, the processing can be continued using a frequency domain processing algorithm, which allows filtering, modulation*, etc.* of the signal, and then reducing it to a time domain signal using the inverse Fourier transform [8]. Figures 7 and 8 show the amplitude and phase diagrams of the original thermogram sequence after processing by the DFT method. The heat map sequence is processed:

$$F_n = \sum_{k=0}^{N-1} \alpha(k) \mathrm{e}^{-j2\pi nk/N} = R_n + jI_n \tag{5}$$

$$A(n) = \sqrt{R_n^2 + I_n^2} \tag{6}$$

$$\phi(n) = \arctan\left(\frac{I_n}{R_n}\right) \tag{7}$$

where $\alpha(k)$ is the value of the (x, y) pixel point in the k^{th} frame of the infrared heat map, n – the serial number following frequency discretization, and R_n and I_n are the real and imaginary components of the transformed complex numbers.

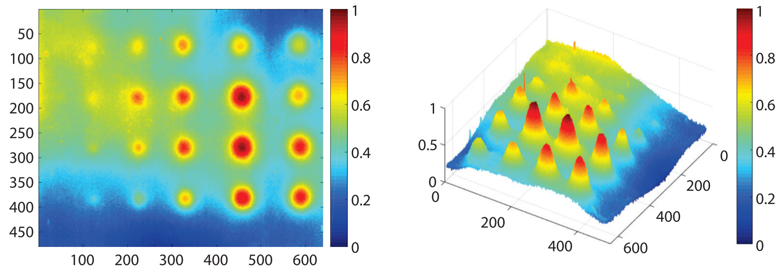

Figure 7. Results of DFT amplitude

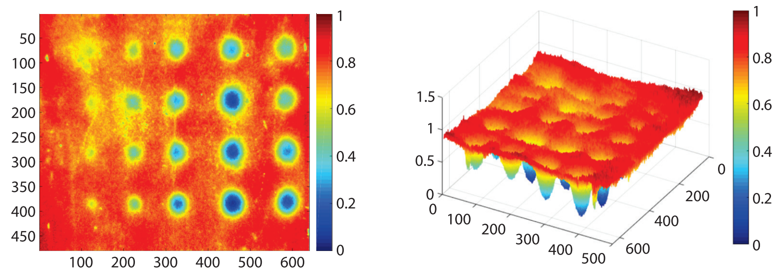

Figure 8. Results of DFT angle

Total harmonic distortion

The total harmonic distortion (THD) borrows a concept from microelectronics that quantifies the noise in the image and applies the total harmonic distortion fast thermal imaging by processing the infrared thermogram [9]:

$$F_{\text{peak}} = F(s) = \frac{q_0}{\mathrm{e}\sqrt{\pi}} \frac{\Gamma(0.5)}{\sqrt{s}} \tag{8}$$

Figure 9 shows a plot of the F_{peak} results obtained from the original thermogram after the THD method and normalization.

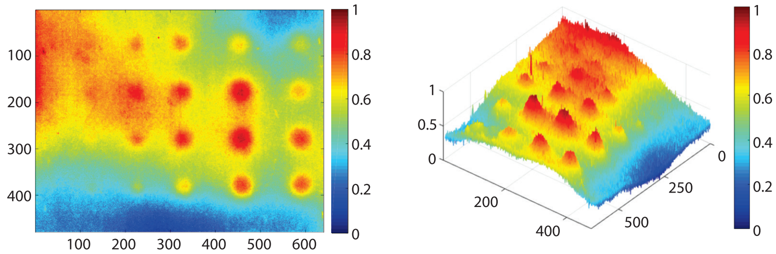

Figure 9. The result of infrared thermogram processed by THD

Algorithm evaluation

In order to compare the influence of the test parameters on the detection results, as shown in fig. 10, the rectangular area at the center of the defect and the rectangular area at the absence of defects are taken to define the SNR for analysis, as shown in eq. (9) [10]. the larger the SNR value, the smaller the influence of noise and the better the ability to detect defects:

$$SNR = \frac{\bar{P}_d - \bar{P}_s}{\sigma_s} \tag{9}$$

where $\bar{P}_d$ is the mean value of the eigenvalues of the defective area, $\bar{P}_s$ – the mean value of the eigenvalues of the defect-free area, σ_s – the standard deviation of the eigenvalues in the defect-free region, and SNR [db] – the signal-to-noise ratio.

The SNR of the best images for each of the aforementioned sequence processing methods was calculated, as shown in fig. 11. For defects with diameters of 10 mm, 8 mm, and 6 mm, the SNR after the THD method was smaller, the SNR after the DFT method was better than the THD method, and the SNR after the PCA method was the largest, so the image sequence processing effect of the PCA method was relatively better.

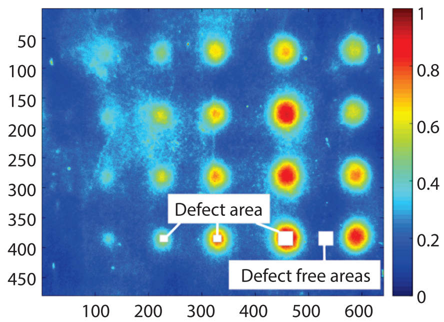

Figure 10. Reference area of SNR

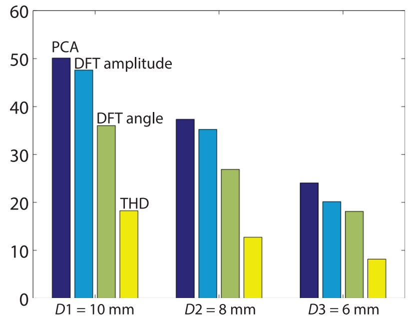

Figure 11. The SNR Comparison chart

Conclusions

In this paper, the zirconia TBC test specimen was prepared, a non-linear frequency modulation infrared thermal imaging detection system was built and tested, the relationship between temperature difference and defect diameter, excitation power, initial frequency and termination frequency was analyzed, and the effects of PCA, DFT, and THD on image sequence processing were compared. The following are the primary conclusions are as follows.

- When the coating thickness is constant, the temperature difference increases with the increase of defect diameter; The temperature difference increases with the increase of excitation power. The temperature difference increases with the decrease of initial and terminal frequencies. Therefore, the defects obtained by appropriately increasing the excitation power and decreasing the modulation frequency during the test are more obvious, thus realizing more effective detection of debonding defects.
- The SNR of PCA method is larger than that of DFT method and THD method through sequence processing of test data. Therefore, the image sequence processing effect of PCA method is better.

Acknowledgment

This project is supported by National Natural Science Foundation of China (Grant No. 51775175), Heilongjiang Provincial Undergraduate University Funded Project of Basic Scientific Research Business Fee (Grant No. 2020-KYYWF-0696), and Heilongjiang Province Natural Science Fund (Grant No. LH2021E088).

Reference

[1] Wang, B., *et al*., Research and Application of Thermal Barrier Coatings for Aeroengine and Gas Turbine Blades, *Aeroengine*, *47* (2021), S1, pp. 25-31
[2] Wang, Q., *et al*., Progress on Heat Insulation Performance of Thermal Barrier Coating, *Journal of Functional Materials*, *44* (2013), 23, pp. 3363-3367
[3] Wang, Z. P., *et al.*, Failure Mechanism, Improvement Method and Future Development Direction of Thermal Barrier Coatings, *Surface Technology*, *50* (2021), 7, pp. 126-137
[4] Li, X. L., *et al*., The Application and Progress of Infrared Thermal Wave Non-destructive Detection Technology, *Non-Destructive Testing*, *37* (2015), 6, pp. 19-23
[5] Chen, D. P., *et al*., Infrared Thermography NDT and Its Development, *Computer Measurement and Control*, *24* (2016), 4, pp. 1-6
[6] Gong, J. L., *et al*., A Study on the SNR Performance Analysis of Laser-Generated Bidirectional Thermal Wave Radar Imaging Inspection for Hybrid C/GFRP Laminate Defects, *Infrared Physics and Technology*, *111* (2020), 2, 103526
[7] RAJIC, N., *et al*., Principal Component Thermography for Flaw Contrast Enhancement and Flaw Depth Characterisation in Composite Structures, *Composite Structures*, *58* (2002), 4, pp. 521-528
[8] Ma, Y. H., *et al*., Discrete Fourier Transform and its Application, *China Modern Educational Equipment*, *13* (2015), 2, pp. 56-58
[9] Shmilovitz, D., *et al*., On the Definition of Total Harmonic Distortion and its Effect on Measurement Interpretation, *IEEE Transactions on Power Delivery*, *20* (2005), 1, pp. 526-528
[10] Tang, Q. J., *et al*., Infrared Micro Thermal Imaging Detection of Micro-crack Defects in Semiconductor Silicon Wafers, *Journal of Heilongjiang University of Science and Technology*, *31* (2021), 2, pp. 177-183

Paper submitted: August 11, 2022
Paper revised: November 10, 2022
Paper accepted: November 22, 2022